AD-A049 327 SHEFFIELD UNIV (ENGLAND) DEPT OF CHEMICAL ENGINEERIN--ETC F/G 21/2
PROGRESS IN MODELLING COMBUSTORS.(U)
1977 P G FELTON, J SWITHENBANK, A TURAN AFOSR-74-2682

UNCLASSIFIED SR-2 AFOSR-TR-77-1297 NL

| OF |
AD
A049 327

END
DATE
FILMED
2-78
DDC

AFOSR-TR- 77-1297

(6)

department of chemical engineering and fuel technology

UNIVERSITY OF SHEFFIELD

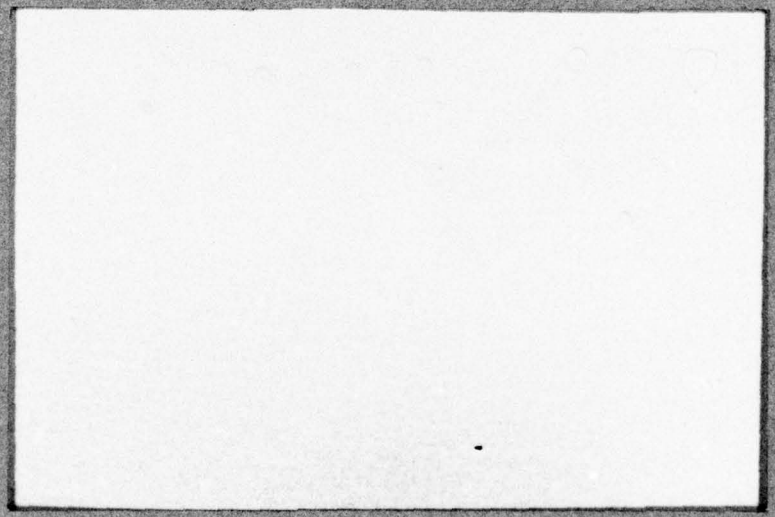

See Form 1473

Progress in Modelling Combustors.

P.G. Felton, J. Swithenbank and A. Turan.

Progress in Modelling Combustors

P.G. Felton, J. Swithenbank and A. Turan

Abstract

Analytical models are required for the design and development of combustors whose applications range from gas turbine engines to industrial boilers. Recent advances in the solution of the problem of predicting the performance of combustors have been based on finite difference and stirred reactor methods.

Three-dimensional finite difference methods were pioneered by Professor Spalding and co-workers and these techniques have been successfully applied to the prediction of gas turbine combustor flow patterns. Due to the limitations of present computers these methods cannot be extended to completely include fuel spray dynamics and realistic chemical kinetics. This difficulty is overcome by using the computed flow patterns to define a network of interconnected stirred and plug-flow reactors. The detailed kinetic scheme presently consists of 13 species undergoing 18 reactions to represent the combustion of hydrocarbon fuels such as kerosine. A model of fuel evaporation is incorporated which assumes the fuel spray to be composed of 21 x 12 μm size ranges, evaporation is calculated using a forced convection model. The mixing of fuel vapour and air is modelled using a micro-mixing parameter, τ_{SD}, based on turbulence dissipation rates. The overall method thus combines 3-D fluid dynamics, turbulent mixing, evaporation and chemical kinetics.

The model has been verified by experiments which show that flow velocity profiles, chemical species (CO, NO etc.) can be successfully computed.

Introduction

Combustion is one of the most difficult processes to model mathematically since it generally involves the simultaneous processes of three-dimensional two-phase fluid dynamics, turbulent mixing, fuel evaporation, radiative and convective heat transfer, and chemical kinetics. In order to design combustors based on fundamental principles, a comprehensive model incorporating

all these factors is required (1). Unfortunately, although we can write down a set of governing differential equations, the solution of these equations is much beyond the capability of present computers and a compromise has therefore been sought. In this study, the approach takes advantage of the fact that there is relatively weak coupling between the fluid dynamic aspects of the flow and the chemical kinetics. That is, the flow pattern is largely defined by the geometry of the combustor and is insensitive to the detailed chemical species present in the flow provided the approximate temperature rise is represented. The calculation is therefore divided into two sections, each of which is within the capabilities of present computers.

It is fair to ask what are the advantages of such a procedure in view of the fact that combustors have been designed and operated for many years without the benefit of these methods. The answer is that combustor development by cut-and-try methods is expensive and does not necessarily produce the optimum answer. Present pressures to minimize both fuel consumption and combustion generated pollution has lead to the need to turn increasingly to fundamental considerations, for example, to help reduce nitric oxide production. A key factor in such solutions is the effective fuel distribution, and this is determined by the fuel preparation technique. It is therefore essential that the model incorporate an accurate representation of the fuel droplet (or particle) size distribution and solves the relevant equations for trajectory and evaporation.

The first stage of the calculation therefore consists of predicting the three-dimensional flow pattern, and here we have extended and applied the finite difference methods pioneered by Professor Spalding and co-workers at Imperial College. The next section of the paper discusses how these methods have been implemented and verified using a typical gas turbine combustor geometry, see Fig.1. In order to include the effect of temperatur rise on the flow pattern, the model includes a crude two step chemical kinetic scheme and a crude droplet evaporation scheme. The relevant output consists of the distribution throughout the combustor of velocity components, turbulent kinetic energy, turbulence dissipation rates, temperature, pressure and heat transfer rates.

The second stage of the calculation derives from chemical plant flowsheet techniques. It consists of a procedure which represents the combustor as a network of interconnected stirred and plug flow reactors, and includes a detailed kinetic scheme for the chemical species to be considered. A more detailed model of the fuel evaporation and mixing rate is also built into this part of the computation since only the fuel which has evaporated and mixed with the air can take part in the chemical reaction. The objective of this stage of the computation is to predict the combustion efficiency and pollution levels produced by the particular combustor design. An important aspect of such a procedure is that it should be capable of predicting the trend of dependence. For example, it is important to be able to predict the effect which a finer fuel spray may be expected to have on the production of nitric oxide at some particular combustor throughput.

The link between the first and second stages of the calculation consists of identifying the appropriate reactor network from the computed flow pattern. The basic hypothesis used for this link is that mixing at the molecular level is carried out by the movement of molecules between turbulent eddies having different concentration. Since the molecules also carry momentum and hence dissipate the turbulence, it is assumed that mixing rate is proportional to turbulence dissipation rate. The output of the first stage (flow pattern) calculation gives the distribution of turbulence dissipation with high values in the vicinity of the jets where air is introduced into the combustor. These regions of high turbulence dissipation thus become well stirred reactors (WSR) of corresponding volume, and the degree of stirring or mixing rate factor τ_{SD} is determined from the total dissipation (or energy transfer) within the reactor. Reactors having low mixing rates are represented as plug flow reactors (PFR) and it is assumed that reactions taking place there are confined to the material which is already mixed. The flow rates and interconnections between the reactors forming the network are determined directly from the overall flow pattern. The link between the two stages of the computation is therefore complete and could be automated in the computer if required, however we have not yet made this step. Indeed the purpose of the present study is to demonstrate the validity of the separate stages.

In some cases, the region in the immediate vicinity of the fuel nozzle is a major source of pollution; since it is unnecessarily extravagant on computer time to study this region in detail using the preceding procedures, a separate axi-symmetrical two phase flow analysis with detailed droplet size distribution representation is used (2), however space precludes the inclusion of this complementary study herein.

Finite Difference Procedure for Flow Pattern Prediction.

The finite difference procedure employed in this work (3) uses the cylindrical polar system of coordinates to predict the complex three-dimensional swirling and reacting flow inside a combustor.

The numerical scheme for solving the governing non-linear equations with arbitrary boundary conditions coupled with mathematical models of turbulence and combustion has the pressure and velocities as the main flow variables; facilities exist to handle both physically-controlled and kinetically controlled reactions and a six-flux radiation model.

The study can undertake problems in Cartesian and cylindrical polar coordinates. Of these two systems the cylindrical-polar coordinates can be regarded as the more general one, for the Cartesian coordinates can be derived from it by siting the flow domain far away from the axis. To simplify the discussion all following equations will be presented in cylindrical polar coordinates with the understanding that the corresponding form of the equations can be readily derived by letting all the r's approach infinity and replacing $r\partial\theta$ by ∂z.

(a) Equations of continuity and momentum.

Continuity:

$$\frac{\partial \rho}{\partial t} + \text{div}\,(\rho \vec{v}) = 0 \qquad (1)$$

u - momentum:

$$\frac{\partial(\rho u)}{\partial t} + \text{div}\,(\rho \vec{v} u - \mu \text{grad} u) = -\frac{\partial p}{\partial x} - \frac{2}{3}\frac{\partial}{\partial x}(\mu \text{div}\vec{v})$$

$$+ \frac{\partial}{\partial x}\left(\mu \frac{\partial u}{\partial x}\right) + \frac{1}{r}\frac{\partial}{\partial r}\left(\mu r \frac{\partial v}{\partial x}\right) + \frac{\partial}{r\partial\theta}\left(\mu \frac{\partial w}{\partial x}\right) \qquad (2)$$

r - momentum:

$$\frac{\partial(\rho v)}{\partial t} + \text{div}(\rho \vec{v} u - \mu \text{grad} v) = -\frac{\partial p}{\partial r} - \frac{2}{3}\frac{\partial}{\partial r}(\mu \text{div}\,\vec{v})$$

$$+ \frac{\partial}{\partial x}\left(\mu \frac{\partial u}{\partial r}\right) + \frac{1}{r}\frac{\partial}{\partial r}\left(\mu r \frac{\partial v}{\partial r}\right) + \frac{\partial}{r\partial\theta}\left[\mu\left(\frac{\partial w}{\partial r} - \frac{w}{r}\right)\right]$$

$$- \frac{2\mu}{r}\left(\frac{\partial w}{r\partial\theta} + \frac{v}{r}\right) + \frac{\rho w^2}{r} \qquad (3)$$

θ - momentum:

$$\frac{\partial(\rho w)}{\partial t} + \text{div}\,(\rho \vec{v} w - \mu \text{grad} w) = -\frac{\partial p}{r\partial\theta} + \frac{\partial}{\partial x}\left(\frac{\mu}{r}\frac{\partial u}{\partial\theta}\right)$$

$$+ \frac{1}{r}\frac{\partial}{\partial r}\left[\mu r\left(\frac{1}{r}\frac{\partial v}{\partial\theta} - \frac{w}{r}\right)\right] + \frac{1}{r}\frac{\partial}{\partial\theta}\left[\frac{\mu}{r}\left(\frac{\partial w}{\partial\theta} + 2v\right)\right]$$

$$- \frac{\rho v w}{r} + \frac{\mu}{r}\left(\frac{\partial w}{\partial r} + \frac{\partial v}{r\partial\theta} - \frac{w}{r}\right) - \frac{2}{3}\frac{\partial}{r\partial\theta}(\mu \text{div}\,\vec{v}). \qquad (4)$$

For the present study:

$$\text{div}\,(\rho \vec{v}\phi) = \frac{1}{r}\frac{\partial}{\partial x}(r\rho u\phi) + \frac{\partial}{\partial r}(r\rho v\phi) + \frac{\partial}{\partial\theta}(\rho w\theta)$$

$$\text{div}\,(\mu \text{grad}\phi) = \frac{1}{r}\left[\frac{\partial}{\partial x}\left(r\mu \frac{\partial\phi}{\partial x}\right) + \frac{\partial}{\partial r}\left(r\,\mu \frac{\partial\phi}{\partial r}\right)\right.$$

$$\left. + \frac{\partial}{\partial\theta}\left(\mu \frac{\partial\phi}{r\partial\theta}\right)\right]$$

In the above equations, u, v and w are the component velocities in the directions x, r and θ respectively; p is the pressure; ρ and μ are respectively the density and viscosity of the fluid mixture.

For turbulent flows which are frequently encountered in combustion studies it shall be assumed that the same equations are also valid provided that one uses time-mean values for all the flow variables and fluid properties and that μ is now the effective viscosity which is the molecular viscosity augmented by the turbulent contribution. The latter is derived at each point from:

$$\mu_t = C_D \rho\, k^2/\varepsilon \qquad (5)$$

where C_D is a universal constant.

The hydrodynamic turbulence model applied here is a two equation model of turbulence known as the k-ε model, Reference (4). It entails the solution of two transport equations for turbulence characteristics namely that of k, the local kinetic energy of the fluctuating motion and ε, the energy dissipation rate. Knowledge of k and ε allows the length scale to be determined and also the effective viscosity (as above) from which the turbulent shear stresses can be calculated.

The differential transport equations for k and ε are as follows:

$$\frac{\partial(\rho k)}{\partial t} + \text{div}\,(\rho \vec{v} k - \Gamma_{k,\text{eff}} \,\text{grad}\, k) = G_K - C_D \rho\varepsilon \tag{6}$$

$$\frac{\partial(\rho \varepsilon)}{\partial t} + \text{div}\,(\rho \vec{v} \varepsilon - \Gamma_{,\text{eff}} \,\text{grad}\, \varepsilon) = (C_1 G_K - C_2 \rho\varepsilon)\frac{\varepsilon}{k} \tag{7}$$

In the above equations the generation term for k, G_K is given by:

$$G_K = \mu_t \left[2 \left\{ \left(\frac{\partial u}{\partial x}\right)^2 + \left(\frac{\partial v}{\partial r}\right)^2 + \left(\frac{\partial w}{r\partial\theta} + \frac{v}{r}\right)^2 \right\} + \left(\frac{\partial w}{\partial x} + \frac{\partial u}{r\partial\theta}\right)^2 + \left(\frac{\partial u}{\partial r} + \frac{\partial v}{\partial x}\right)^2 + \left(\frac{\partial w}{\partial r} + \frac{\partial v}{r\partial\theta} - \frac{w}{r}\right)^2 \right] \tag{8}$$

C_D, C_1 and C_2 are constants. $\Gamma_{k,\text{eff}}$ and $\Gamma_{\varepsilon,\text{eff}}$ are the effective exchange-coefficients.

Recommended values for the constants appearing in the above equations are:

C_D	C_1	C_2
0.09	1.43	1.92

(9)

(b) Reaction Models

Conservation equation for a chemical species j:

$$\frac{\partial(\rho m_J)}{\partial t} + \text{div}\,(\rho \vec{v} m_j - \Gamma_J \,\text{grad}\, m_J) = R_J$$

where m_J is the mass fraction of the chemical species j, R_J the mass rate of creation of species j by chemical reaction, per unit volume, and Γ_J is the exchange coefficient.

In a multi component system simplifications can be introduced through the use of the concept of a simple chemically reacting system. This model is based on the assumptions that: the fuel and air react chemically in a unique proportion; that the effective diffusivities of all chemical species are equal; that the reaction is a single step with no intermediate compounds.

These suppositions make it possible to solve only one equation for the variable f defined as the mass fraction of fuel in any form (burnt or unburnt) for diffusion flames and two equations with variables m_{fu} and f respectively for the kinetically influenced flames.

The quantity f is defined mathematically as:

$$f = (\nu - \nu_{ox})/(\nu_{fu} - \nu_{ox}) \tag{10}$$

and $\nu_{ox} \equiv -(m_{ox}/s)_{inlet}$

$\nu_{fu} = (m_{fu})_{inlet}$; $s \equiv$ stoichiometric constant.

The quantities $(m_{fu})_{inlet}$ and $(m_{ox})_{inlet}$ are the mass fraction of fuel and oxygen in the fuel and oxidant stream respectively.

The mass fractions of fuel (for the diffusion controlled case) and oxygen are related to the mixture fraction according to:

$0 < f \leq f_{st}$: $\quad m_{fu} = 0$

$\quad m_{ox} = (1 - f/f_{st})\, m_{ox\ inlet}$

$1 > f \geq f_{st}$: $\quad m_{fu} = (f - f_{st})/(1-f_{st})$

$\quad m_{ox} = 0$

In the above equations f_{st} is the stoichiometric value of the mixture fraction and is given by:

$$f_{st} = 1/\left[1 + s\left(\frac{m_{fu}}{m_{ox}}\right)_{inlet}\right] \tag{12}$$

The mass fraction of nitrogen and the combustion products are treated similarly.

The influence of turbulence on reaction rates is taken into account by employing the eddy break up model of Spalding (5).

The reaction rate in this case is taken to be the smaller of the two expressions given by the familiar Arrhenius formulation and the eddy break up model. The latter is conveniently described as

$$R_{fu'EBU} = -C_R \rho g^{\frac{1}{2}} \varepsilon/k \qquad (13)$$

where C_R is a constant and g represents the local mean square concentration fluctuations.

(c) Radiation Effects

The effect of radiation in the mathematical model are accounted for by reference to the six-flux model of radiation. The differential equations describing the variations of the fluxes are: Reference (6)

$$\frac{d}{dr}(rI) = r\left[-(a+S_1)I + \frac{J}{r} + aE + \frac{S_1}{6}(I+J+K+L+M+N)\right]$$

$$\frac{d}{dr}(rJ) = r\left[(a+S_1)J + \frac{J}{r} - aE - \frac{S_1}{6}(I+J+K+L+M+N)\right]$$

$$\frac{d}{dx}(K) = -(a+S_1)K + aE + \frac{S_1}{6}(I+J+K+L+M+N) \qquad (14)$$

$$\frac{d}{dx}(L) = (a+S_1)L - aE - \frac{S_1}{6}(I+J+K+L+M+N)$$

$$\frac{dM}{rd\theta} = -(a+S_1)M + aE + \frac{S_1}{6}(I+J+K+L+M+N)$$

$$\frac{dN}{rd\theta} = (a+S_1)N - aE - \frac{S_1}{6}(I+J+K+L+M+N)$$

where:

I - radiation flux in the direction of positive r.
J - radiation flux in the direction of negative r.
K - radiation flux in the direction of positive x.
L - radiation flux in the direction of negative x.
M - radiation flux in the direction of positive θ.
N - radiation flux in the direction of negative θ.
a - absorption coefficient.
S_1 - scattering coefficient.

$E \equiv \sigma T^4$ black body emissive power at the fluid temperature;

$\sigma \equiv$ Stefan-Boltzmann constant.

The composite fluxes defined as:

$$R^X \equiv \frac{1}{2}(I + J)$$

$$R^Y \equiv \frac{1}{2}(K + L) \qquad (15)$$

$$R^Z \equiv \frac{1}{2}(M + N)$$

are employed to eliminate I, J, K, L, M and N from the previous equations to yield three second-order ordinary differential equations.

(d) Solution procedure.

The previous governing partial differential for mass, momentum, energy and species concentrations are elliptic in nature and can be conveniently presented in the general form:

$$\frac{\partial(\beta\phi)}{\partial t} + \text{div}\,(\beta\vec{v}\phi - \Gamma\,\text{grad}\phi) = S_2 \qquad (16)$$

In the above equation ϕ identifies the dependent variable; β is identically equal to either the mixture density ρ or zero; Γ is the appropriate exchange coefficient for the variable ϕ; and S_2 is the source term.

Table (1) summarizes the expressions for the symbols β, Γ and S_2.

The equations are first reduced to finite difference equations by integrating over finite control volumes (Reference 3) and then solved by a procedure described in detail in Reference (7) for three dimensional parabolic flows.

It will be sufficient for the purposes of this paper to summarise the main features of the solution procedure.

The numerical scheme is a semi-implicit iterative one which starts from given initial conditions for all the variables and converges to the correct solution on the completion of a number of iterations.

Each iteration performs the following steps:

i) The u, v and w momentum equations are solved sequentially with guessed pressures.

ii) Since the velocities at this stage do not satisfy the continuity equation locally, a "Poisson-type" equation is derived from the continuity equation and the three linearised momentum equations. This "Poisson" equation is then solved for corrections to the pressure field and the consequent corrections of the three velocities. (SIMPLE algorithm).

iii) The k and ε equations are then solved using the most up to date values of velocities.

iv) The iteration is completed upon solution of the concentration and all the remaining equations.

One point to note here is the implementation of the cyclic boundary condition in the θ direction compatible with the nature of the swirling flows

(e) Results of the Flow Analysis (Computed and Experiment).

A simple gas turbine combustor, Fig.2., was used to study the comparison between computer flow predictions and the experimentally observed values.

The air stream through the swirler enters the chamber with finite swirl velocity while the primary, secondary and the dilution flows are each injected through 6 equally spaced circular orifices on the periphery giving rise to the three-dimensional nature of the problem.

There were no wall cooling slots and the combustor was operated in a large plenum so that no axial velocity components were included in the radial jet flows. The finite difference grid network reported here consisted of 27 transverse planes, 7 radial planes and 18 circumferential surfaces (Fig.2.).

The cyclic boundary condition mentioned above, can be employed to consider only a 60° sector with the particular input data given below:

Total air flow rate = 0.1275 kg/sec.

Swirler:

Air flow rate = 0.0016575 kg/sec for the 60° sector.

Fuel flow rate = 0.0 (cold), 0.000178 (hot)

Swirl = 0.8

Inlet temp. = 351 K

Axial velocity = 27.6 m/s

Swirl velocity = 14 → 22 m/s (Forced vortex, w ∿ radius)

Injection Details:

Primary Injection.

Flow rate = 0.005421 kg/sec. per orifice.

Injection velocity = 138.90 m/sec.

Secondary Injection.

Flow rate = 0.006355 kg/sec. per orifice.

Injection velocity = 139.1 m/sec.

Dilution.

Flow rate = 0.007820 kg/sec. per orifice.

Injection velocity = 138.7 m/sec.

Injection temperature (for all ports) = 351 K.

It is difficult to represent the full detail of the flow in a paper such as this, therefore a few profiles have been selected to indicate the character of the results.

In Fig.3, the calculated radial velocities are shown at two radii for a longitudinal cross-section. The decay of the radial jet velocity and the small radial outflow between the holes will be noted.

In Fig.4. the axial velocities are shown for a number of axial locations. As in the case of Fig. 3, this graph is for a section through the centre of the holes, and the radial expansion of the jets is clear. Particularly noteworthy is the negative fl[illegible]oundary in the primary zone, which indicates the boundary of the recirculation zone. This location of the recirculation zone was simply verified on the test rig by introducing a sodium tracer into the flame. When the tracer was introduced into the recirculation zone, the whole exit flow was coloured yellow, whereas only a small region was yellow when it was introduced outside the recirculation zone. The axial velocity profile at the exit will be discussed in more detail below.

Fig.5. shows the radial velocity profile at three radii plotted at a cross-section through the primary jets. The slight skewness caused by the swirl can be detected, and the swirl velocity profile is also plotted on the same figure.

In Fig.6 the turbulence dissipation contours are plotted for an axial cross-section. Two sets of contours are shown corresponding to sections through the jets and at the edge of the jets respectively. This figure clearly illustrates the fact that dissipation (and mixing) is concentrated in the vicinity of the jets, and corresponds to the stirred reactor locations.

It is difficult to make accurate three dimensional velocity measurements in a small combustor. The problem is that a 5 or 7 hole spherical probe occupies too much space in the strong shear flow within the combustor. It was therefore decided that the best comparison location between the predicted and measured flow fields would be obtained at the combustor exit. In Fig.7a, these experimental and theoretical exit axial flow profiles are plotted and it can be seen that the agreement is remarkably good. In Fig.7b, the more complex factor of exit turbulence intensity is plotted and again experimental and theoretical values are compared. The experimental values were obtained with a photon-correlation laser doppler anemometer. Again the agreement is remarkably good considering the difficulty of the experiment and the complexity of the prediction, however the results suggest that the model slightly overestimates the turbulence. In Fig.7c the exit temperature profiles are compared and again the model successfully predicts the poor exit traverse with a temperature minimum close to the axis.

Stirred Reactor Modelling.

As pointed out previously, the second stage of the overall combustor modelling procedure is to model the flowfield by an appropriate network of stirred reactors. Consequently a sub-model is required for a Well Stirred Reactor, WSR, (N.B. not perfectly stirred) which includes the internal processes of fuel evaporation, mixing and complex chemical kinetics. It is possible to use "global" reaction rate data in such a system to predict combustion performance and combustor stability (ref.8), however, if prediction of pollutant emissions is to be attempted then detailed chemical kinetic schemes are required. In addition, to model those sections of the flowfield where no mixing is taking place, a Plug Flow Reactor model is required, this can be achieved by a sequence of differentially small W.S.R.s.

Previously stirred reactor models of combustors have been mainly confined to homogeneous combustion with "global" reaction kinetics (ref.9), although

Gaseous phase mass balance $\dot{m}_1 - \dot{m}_2 + \dot{FE} = dm/dt$ (20)

Liquid phase mass balance $\dot{\epsilon}_1 - \dot{\epsilon}_2 - \dot{FE} = d\epsilon/dt$ (21)

Mass balance on the unmixed fluid in the gaseous phase

$$d(m\,\phi_u)/dt = \dot{m}_1\,\phi'_u - \dot{m}_2\,\phi_u - m\,\phi_u/\tau_D + \dot{FE}$$

$$\therefore \quad m\frac{d\phi_u}{dt} + \phi_u\frac{dm}{dt} = \dot{m}_1\,\phi'_u - \dot{m}_2\,\phi_u - \frac{m\phi_u}{\tau_D} + \dot{FE} \tag{22}$$

Using (22)

$$m\frac{d\phi_u}{dt} = \dot{m}_1\,(\phi'_u - \phi_u) - \frac{m\phi_u}{\tau_D} + \dot{FE}\,(1 - \phi_u)$$

At the steady state $\frac{dm}{dt} = \frac{d\phi_u}{dt} = 0$

$$\text{Thus} \quad \frac{m}{\dot{m}_1} = \frac{m}{(\dot{m}_2 - \dot{FE})} = \frac{m/\dot{m}_2}{(1 - \dot{FE}/\dot{m}_2)} = \frac{\tau_s}{(1-\beta)} \tag{23}$$

where $\beta = \dot{FE}/\dot{m}_2$ (24)

$$\therefore \quad \phi_u = \frac{\phi'_u(1-\beta) + \beta}{(1 + \tau_{SD})} \tag{25}$$

where $\tau_{SD} = \tau_s/\tau_D$ (unmixedness parameter)

Thus for a given $\dot{FE}$, τ_{SD} and feed conditions (25) defines the proportion of the steady state reactor gas phase which is unmixed. Therefore the reactor composition prior to reaction may be expressed as follows:-

$$C_f^* = \phi_u\,\omega_f + (1 - \phi_u)\,\gamma_f^*$$

$$C_{O_2}^* = \phi_u\,\omega_{O_2} + (1 - \phi_u)\,\gamma_{O_2}^*$$

$$C_{N_2}^* = \phi_u\,\omega_{N_2} + (1 - \phi_u)\,\gamma_{N_2}^*$$

$$C_{CS}^* = (1 - \phi_u)\,\gamma_{CS}^*$$

encouraging results were obtained within the limitations of this approach (ref.8). Evaporation effects were later included with some success (ref.10).

Although the three processes of evaporation, mixing and reaction must occur simultaneously in a combustor it is convenient to consider that in a steady state condition these processes occur in series. Thus the fuel must first evaporate, then mix and finally react. This approach allows us to calculate the reactor gaseous phase composition after evaporation and mixing have taken place, this constitutes the homogeneous feed to the reactor. A general combustion scheme which summarizes this is shown in table 1.

The feedstream to, or product stream from any reactor is assumed to be composed of any or all of the eight species in the above scheme. Figure 8 shows the composition of the general two phase steady state reactor with the liquid phase shown coalesced for convenience. Transfer from the liquid phase to the gas phase is represented by the mean fuel evaporation rate, $\dot{FE}$. In addition it is assumed that the mean residence time of each phase in the reactor is the same. This assumption is incompatible with the existence of a relative velocity between the gas and the fuel droplets but greatly simplifies the analysis and calculation of fuel distribution around any particular reactor network. It is not essential to assume this however, and the analysis could be modified to incorporate unequal phase residence times. Transfer of fluid from the unmixed state to the mixed state is assumed to take place at the following rate:-

$$(\text{mass of unmixed fluid})/\tau_D$$

where τ_D is the characteristic turbulence dissipation time.

$$\text{Total reactor mass} = m + \varepsilon \tag{17}$$

$$\tau_s = m/\dot{m}_2 = \varepsilon/\dot{\varepsilon}_2 \tag{18}$$

Using (17)

$$\tau_s = V/(\dot{m}_2/\rho_G + \varepsilon_2/\rho_2) \tag{19}$$

N.B. $$\omega_f + \omega_{O_2} + \omega_{N_2} = \gamma^*_f + \gamma^*_{O_2} + \gamma^*_{N_2} + \gamma^*_{CS} = 1 \qquad (26)$$

The concentrations of the unmixed species can be obtained by performing the relevant species mass balances. For example, unmixed fuel vapour mass balance is as follows:-

$$\frac{d(m\phi_u\,\omega_f)}{dt} = \dot{m}_1\phi'_u\,\omega'_f - \dot{m}_2\,\phi_u\,\omega_f + \dot{FE} - \frac{m\,\phi_u\,\omega_f}{\tau_D} \qquad (27)$$

At the steady state $d(m\,\phi_u\,\omega_f)/dt = 0$

$$\therefore \quad m\,\phi_u\,\frac{d\,\omega_f}{dt} + m\,\omega_f\,\frac{d\phi_u}{dt} + \phi_u\,\omega_f\,\frac{dm}{dt} = 0$$

As $d\omega_f/dt = 0$

$$(1-\beta)\phi'_u\,\omega'_f - \phi_u\,\omega_f + \beta - \phi_u\,\omega_f\,\tau_{SD} = 0$$

$$\therefore \quad \omega_f = \frac{\phi'_u\,(1-\beta)\,\omega'_f + \beta}{\phi_u\,(1+\tau_{SD})} = \frac{\phi'_u\,(1-\beta)\,\omega'_f + \beta}{\phi'_u\,(1-\beta) + \beta} \qquad (28)$$

using (25)

Similarly:- $$\omega_{O_2} = \frac{\phi'_u(1-\beta)\,\omega'_{O_2}}{\phi'_u(1-\beta) + \beta}$$

and $$\omega_{N_2} = \frac{\phi'_u\,(1-\beta)\,\omega'_{N_2}}{\phi'_u(1-\beta)+\beta}$$

The expressions for the intermediate concentrations of the mixed reactants and combustion products are obtained by performing similar mass balances on the mixed portion of the reactor gas phase. For example, the mixed fuel vapour mass balance is as follows:-

$$\frac{d(m\,(1-\phi_u)\,\gamma^*_f)}{dt} = \dot{m}_1\,(1-\phi'_u)\gamma'_f - \dot{m}_2\,(1-\phi_u)\gamma^*_f + \frac{m\,\phi_u\,\omega_f}{\tau_D} \qquad (29)$$

Since $\frac{d\gamma^*_f}{dt} = 0$

$$(1-\beta)(1-\phi'_u)\gamma'_f - (1-\phi_u)\gamma^*_f + \phi_u\,\omega_f\,\tau_{SD} = 0$$

$$\therefore \quad \gamma^*_f = \frac{(1-\beta)(1-\phi'_u)\gamma'_f + \phi_u\,\omega_f\,\tau_{SD}}{(1-\phi_u)}$$

Using (25) and (28)

$$\gamma^*_f = \frac{(1-\beta)(1-\phi'_u)(1+\tau_{SD})\gamma'_f + \tau_{SD}(\phi'_u(1-\beta)\omega'_f + \beta)}{(1-\beta)\,(1-\phi'_u) + \tau_{SD}} \tag{30}$$

Similarly:-

$$\gamma^*_{O_2} = \frac{(1-\beta)(1-\phi'_u)(1+\tau_{SD})\gamma'_{O_2} + \tau_{SD}\,\phi'_u(1-\beta)\,\omega'_{O_2}}{(1-\beta)\,(1-\phi_u) + \tau_{SD}}$$

$$\gamma^*_{CS} = \frac{(1-\beta)(1-\phi'_u)(1+\tau_{SD})\gamma'_{CS}}{(1-\beta)(1-\phi'_u) + \tau_{SD}}$$

Having defined the intermediate composition of the gaseous phase, i.e. after mixing and evaporation, two further balances must be made to determine the final reactor composition. These are the species and energy balances for the PSR for the steady state. During the reaction stage the mixed gaseous phase concentrations, γ^*, are transformed to the final concentration γ; the unmixed gas phase concentrations, ω, do not change of course although they do contribute to the physical properties of enthalpy, specific heat and density.

Chemical reaction, mixed species mass balance:-

$$\frac{\dot{m}_2}{\rho_G\,V\,W_i}(\gamma^*_i - \gamma_i)(1-\phi_u) + \dot{p}_i = 0 \tag{31}$$

where i = 1, MT, MT = total number of mixed gaseous species.

Chemical reaction, gas phase energy balance:-

$$\frac{\dot{m}_2}{\rho_G \, V \, W_i} \sum_{i=1}^{MT} (\gamma_i^* \, h_i^* - \gamma_i h_i)(1-\phi_u) + \frac{\dot{m}_2}{\rho_G \, V \, W_i} \sum_{i=MT+1}^{NT} \omega_i (h_i^* - h_i)\phi_u = \dot{H}_L \tag{32}$$

$\dot{H}_L = 0$ for adiabatic operation.

The species kinetic production term is given by:-

$$\dot{p}_i = \sum_{j=1}^{NR} (\alpha_{ij} - \delta_{ij})(F_j - B_j) \tag{33}$$

The forward and backward reaction rates are related to the reactor gas phase species concentrations by the following:-

$$F_j = f_j \, X_j^{\sigma_j} \prod_{i=1}^{MT} \left(\rho_G \, (1-\phi_u) \, \gamma_i / W_i \right)^{\delta_{ij}} \tag{34}$$

$$B_j = b_j \, X_j^{\sigma_j} \prod_{i=1}^{MT} \left(\rho_G \, (1-\phi_u) \, \gamma_i / W_i \right)^{\alpha_{ij}} \tag{35}$$

where X_j is a third body in a dissociation reaction.

$$X_j = \sum_{i=1}^{MT} d_{ij} \left((1-\phi_u) \, \gamma_i / W_i \right) \tag{36}$$

The forward reaction rate constants are:-

$$f_j = A_j \, T^{n_j} \exp(-E_j/RT) \tag{37}$$

The backward reaction rate constants are fixed by the equilibrium constants:-

$$b_j = f_j \, K_j \sum_{i=1}^{MT} (\delta_{ij} - \alpha_{ij}) \tag{38}$$

$$K_j = \exp\left(- \sum_{i=1}^{MT} (\alpha_{ij} - \delta_{ij})\, F_i^{o}/RT \right) (RT) \qquad (39)$$

The system of equations is completed with the equation of state:-

$$P = \rho_G \frac{R}{W} T = \rho_G\, RT \sum_{i=1}^{MT} (1-\phi_u) \frac{\gamma_i}{W_i} + \rho_G\, RT \sum_{i=MT+1}^{NT} (\phi_u \frac{\omega_i}{W_i}) \qquad (40)$$

The final reactor gas phase composition has thus been defined and the final overall concentrations may be expressed as follows:-

$$C_f = \phi_u\, \omega_f + (1 - \phi_u)\, \gamma_f \qquad (41)$$

and similarly for the other species.

The complete set of equations characterises a heterogeneous stirred reactor in steady state operation, they reduce to the equations for the homogeneous case if β is set to zero. These equations are very non-linear due to the exponential dependence of the reaction rates in temperature, additionally FE is a complex function of temperature and staytime, τ_s, hence the WSR equations must be solved iteratively. The technique used is based on the numerical method PSR solution developed by Osgerby (ref.11), in which a Newton-Raphson correction procedure is employed to converge onto the PSR solution, from an initial guess. The data required for the solution are a kinetic scheme, rate data, thermodynamic data, feed conditions and an initial guess. The initial guess is provided by an equilibrium calculation and the kinetic scheme used is shown in table 2.

In order to calculate fuel evaporation rates a timestep technique was devised, the spray is assumed to consist of 21 size intervals each of 12 μ, each of which is represented by the interval mean diameter. The percentage of the fuel spray remaining unevaporated at any elapsed time decreases non-linearly with time, therefore the evaporation rate of the spray is not constant through the reactor. The spray mean evaporation rate is obtained by calculating the total fuel evaporated during the staytime in the reactor and dividing by the staytime. Initially the droplets have a velocity relative

to the gas stream, however as the drag forces acting on the droplets are inversely proportional to the diameter the small droplets rapidly assume the local gas velocity whereas the larger droplets tend to retain their own velocity. There are two modes of combustion possible for an evaporating fuel droplet; droplet diffusion flames and droplet wake flames. The wake flames are generally blue due to good mixing prior to combustion whereas diffusion flames are typically yellow due to soot formation. The velocity necessary to cause a transition from diffusional to wake burning is a strong function of the local oxygen concentration and falls to zero at oxygen concentrations in the range 14 - 16%, thus at such oxygen levels a diffusion flame cannot exist if there is any relative velocity. This is generally the case in gas-turbine combustion. Using the evaporation model of Wise et al (ref.12) we can derive the static evaporation rate:

$$\dot{m}_E = \frac{4 \pi \lambda r_L}{\bar{C}_p} \ln (1 + B_{ev}) \qquad (42)$$

where $B_{ev} = \bar{C}_p (T_\infty - T_L)/L$

and $\lambda = 1.432 \times 10^{-5} \bar{C}_p (T - 44.67)^{2/3}$ W m^{-1} K^{-1}

To allow for the effects of droplet dynamics an empirical correlation of the type suggested by Frössling is used (13):-

$$\dot{m}_{E,F} = \dot{m}_E (1 + 0.244 \, Re^{\frac{1}{2}}) \qquad (43)$$

where $Re = \frac{2 v_{rel} r \rho_G}{\mu_G}$ (43)

In order to incorporate drag effects into the model an expression is required for the acceleration experienced by an individual droplet, the expression derived by Vincent (14) is used:-

$$\frac{d v_{rel}}{dt} = \frac{3 C_D \rho_a v_{rel}^2}{8 r \rho_L} \qquad (44)$$

where $C_D = 0.48 + 28/Re^{.85}$

The only information needed to allow calculation of the evaporation rate is the initial droplet size distribution and the droplet initial velocity, these are normally provided by correlations derived experimentally for the atomizer in use. In our studies, we use the laser diffraction dropsize distribution meter which we have developed. to characterize the spray accurately (15).

Before vaporized fuel and oxidant can react, the respective molecules must be brought into intimate contact, the physical processes involved are termed mixing. Mixing is important under combustion conditions since it is usually the rate determining step, however it is the most difficult process to model mathematically. The principle source of mixing energy in a gas turbine combustor is the pressure loss across the turbulence generator, the can. Since the velocity and concentration fluctuations decay simultaneously it is proposed that the degree of mixing is equal to the degree of turbulence dissipation within the flow system. An energy balance is performed:-

Pressure drop across baffle	=	Energy "held" in flow velocity profile	+	turbulence kinetic energy	+	dissipation energy
$\Delta P/q$	=	KE_{av}/q	+	$3(u'/\bar{U})^2$	+	D/q

$(q = \frac{1}{2}\rho\bar{U}^2)$ (45)

It is proposed that a characteristic dissipation time $\tau_D = C^* \ell_e / u'_{max}$, where C^* = constant (unity), ℓ_e = mean size of energy containing eddies (0.2 λ), u'_{max} = maximum value of the r.m.s. velocity fluctuations. But $\tau_s = X/\bar{U}$ ($X \simeq 10\ \lambda$) $\therefore$ $\tau_{SD} = 50\ (u'/\bar{U})_{max}$, thus using the energy balance (45), this yields $\tau_{SD} = 50\ (\Delta P/3q)^{\frac{1}{2}}$.

Thus the unmixedness parameter, τ_{SD}, used from equation 25 onwards can be related to the system geometry. This parameter has high values for good mixing (> 200) and the values (< 5) cause "blowout" due to inadequate mixing (fig.9). A mathematical model of each process has now been described and these are combined using the equations derived earlier (17 → 41). The equations are solved in the following way, firstly a gas temperature is estimated so that an initial evaporation rate for the reactor can be calculated. Then using the above equations the homogeneous feed to a reactor can be calculated and an equilibrium calculation performed to

generate the atarting values for the iterative calculation. Several iterations of the chemical species equations are performed until the mass convergence test is satisfied, then the energy convergence test is applied. If this is not satisfied then the temperature is corrected by $(H - H)/C_p$ followed by recalculation of the fuel evaporation rate and homogeneous feed condition, after which the Newton-Raphson scheme for solving the chemical species equations is re-entered. It was found that if the fuel evaporation rate was recalculated every time the temperature was corrected then a slight instability is introduced into the iteration, therefore the evaporation rate is only calculated for the first ten iterations by which time the correction is less than 5K.

We have now derived a method for solving an individual reactor; we have to devise a sequence of reactors to represent the combustor under consideration. There are several methods which can be used to determine these sequences:-a)Qualitative observations of combustor performance, e.g. for a typical gas turbine combustor this leads to a series model consisting essentially of a stirred reactor followed by a plug flow reactor. b)The distribution of "macro scale mixing", derived from theoretical and experimental tracer response functions (e.g. water modelling and Argon tracer studies).c) The distribution of "micro mixing" energy within the flow; in this method the stirred reactors are placed in the flow regions where high levels of turbulence energy exist. As already discussed above, the 3-D finite difference procedure is used to determine flow patterns and turbulent energy distribution and hence derive the volumes, flow rates and inter-connections of the appropriate stirred reactor network. An example of a reactor model of a gas turbine combustor is shown in fig.10.

As a simple illustration of the stirred reactor network approach we will discuss its application to a novel design of "blue flame", low pollution burner built at Sheffield (fig.11). Air is added via a Coanda ejector, which causes controlled recirculation of combustion products thus reducing the oxygen concentration in the vicinity of the spray leading to wake burning. The isothermal burner flow pattern was determined by hot wire anemometry measurements. (fig.12). The general flow pattern under burning conditions was assumed to be the same as that under isothermal conditions although flowrates were corrected for density effects. Since the mean

residence time in the Coanda throat is small, no stable combustion can take place there, and the throat is assumed to be an isothermal mixer of atomized spray, feed air and recirculated gases. WSR1 is the main flame zone, its volume is set equal to that of the truncated cone bounded by the dotted line (240 cm^3). The unmixedness parameter, τ_{SD}, for this reactor was estimated to be 300, i.e. virtually perfect mixing. The secondary flame zone is represented by a poorly mixed WSR2 (volume 280 cm^3), this WSR2 was estimated to have a τ_{SD} of 10, (fig. 13). A cooling of the recirculation flow around the narrow coanda unit annulus is to be expected and was apparent from temperature measurements carried out. Consequently a heat exchanger unit was incorporated into the recycle path to take account of this (Fig.14). The kinetic scheme used for the calculations was that referred to earlier, table 2, the rate of reaction 1 is given by:-

$$-\frac{d[C_{12}\ H_{24}]}{dt} = 5.52 \times 10^8 . \exp(-12900/T) . [C_{12}\ H_{24}]^{\frac{1}{2}} . [O_2] . P^{-0.825} \quad (50)$$

In the experimental system water was condensed in the sampling system therefore for comparison purposes the predicted water concentration was reduced by a factor of 10 and all other concentrations adjusted accordingly. The initial size distribution was described by the Rosin-Rammler expression (fig.15), the ·Rammler parameters were related to the fuel injection pressure and atomizer fuel flow number using correlations of the type suggested by Bowen and Joyce (ref.16) based on our own experimental results. The spray initial velocity was calculated using discharge coefficients based on Tipler's results (ref.17), assuming that all the droplets were projected with the same initial velocity.

Results of the Stirred Reactor Analysis (Computed and Experiment).

The predicted values of NO, CO and temperature at the burner exit (after WSR2) are plotted against airflow rate (and hence ϕ) for a given set of operating conditions (Figs.16,17,18,table 3) with the corresponding experimental values. For each of these variables the correct trends and order of magnitude is predicted and in the case of NO and CO the agreement is particularly good. Work is still in progress to extend the computed results to rich mixtures and these will be reported in due course. The

temperature predicted is generally larger than the measured temperature, by up to 200 K, this is due to the measured temperature (by a simple bare thermocouple) not having been corrected for heat losses. The effect of fuel pressure on NO emissions is shown in fig.19 (table 4), again very good agreement for both trend and magnitude was obtained.

Discussion.

The major effort in these studies has been to reduce the computer time to manageable proportions while retaining realistic combustor configurations, and in this endeavour we have been relatively successful. In the finite difference procedure, an obvious variable is the number of nodes on the grid representing the flow field. Preliminary studies showed that a grid much coarser than that used here was inadequate to represent the gas turbine combustor flow field, and similar comments would apply, for example, to an industrial multi-orifice gas-fired tunnel burner. However the system could be simplified considerably if the flow were axi-symmetric, as then only two dimensions appear in the analysis.

A major weakness of the finite difference procedure is the mathematical representation of the turbulence as isotropic, whereas in the important jet flow region it is undoubtedly anisotropic. The significance of this fact is difficult to ascertain since it is probably compensated by the values of the coefficients used in the analysis. The fact that these same coefficients give analytical results in reasonable agreement with a wide range of experiments gives confidence in their use in the systems described here. It is anticipated that even more sophisticated turbulence models can be used in the same basic procedure, as they become available.

The finite difference procedure typically evaluates about twenty partial differential equations giving the values of about twenty variables at each of 3402 grid points. The computer time (ICL 1906S) for convergence is about 2 hours for each case. Separate studies have shown that the fuel spray must be divided into more than about 20 size ranges if it is to be accurately represented in calculations, and if incorporated into the finite difference procedure to this precision it would almost double the number of equations to be solved at each grid point, as well as dramatically increasing the storage requirement. The computer time would then increase to the point where the costs could not be justified even if the computer

power and time were available. Similar considerations apply to the inclusion of a full chemical kinetic scheme into the finite difference flow field analysis, since it has been found that about 20 reactions is the minimum which will adequately represent the combustion process if pollutants are to be predicted. We therefore conclude that the overall procedure proposed here is about the simplest that can adequately represent all the important physical and chemical factors controlling the behaviour of a real combustor.

The most important factor yet to be determined in the stirred reactor model is the coefficient of the mixedness factor τ_{SD}. At present, this coefficient is assumed to be unity, however there is hope that it can be determined more accurately by experiments in which the probability density distribution of the concentration fluctuations are measured. An appropriate simplified analysis is given by Pope in Reference 18. Fortunately the performance of most combustors is not very sensitive to this coefficient.

A further weakness of the stirred reactor program is that it cannot, at present, predict the formation and agglomoration of soot. This problem can be approached from two directions. In the first, we assume that soot is an undesirable product from gas turbine combustors, for instance, and the foregoing design procedure may therefore be used to avoid the local rich conditions under which soot is formed. In the second, more research is needed to determine the appropriate rate equations for soot formation, and these equations may then be incorporated into the existing computer program with a simple change in the input data. If the fuel to be employed were residual oil or coal which burn with a more complex process than simple evaporation, then the appropriate module of the computer program would have to be modified. However the modular nature of the program and simple physical form of the variables allow such changes to be made relatively easily.

Before all the techniques reported above can be applied with confidence, much more comparison with experiment is required, perhaps leading to a refinement in the procedure. This study thus reports a phase of progress on a steadily evolving subject.

Conclusions

1. The problem of mathematically modelling combustion systems has been approached by a combination of finite difference and stirred reactor network methods.

2. The finite difference model predicts the flow and turbulence field and provides the data for setting up the stirred reactor network.

3. The stirred reactor network model incorporates unmixedness and fuel evaporation and predicts the combustion efficiency and pollutant production.

4. Experiments so far carried out have verified that the flow profiles and chemical species (CO, NO etc.) can be successfully predicted.

5. Further work is needed to verify the method over a wider range of combustors and operating conditions.

6. This study presents a phase of progress in a complex but steadily evolving subject.

Acknowledgement

Financial support for this work has been received from the Science Research Council and the USAF European Office of Scientific Research under Grant No. 74 - 2682. This support is gratefully acknowledged. The authors also wish to acknowledge the valuable discussions with Professor Spalding who also made the basic finite difference program available to us. Without this help and assistance from Dr. Srivatsa the first part of this work would not have been feasible. The contributions of Dr. D.S. Prior to the stirred reactor modelling, and Malvern Instruments in making available the photon-correlation anemometer are also gratefully acknowledged.

NOMENCLATURE

i) Finite difference equations

a	Absorption coefficient for radiation.
C_1, C_2, C_D	Constants in the turbulence model.
C_R	Constant in the eddy break-up model.
E	Black body emissive power.
g	Mean square concentration fluctuation of fuel species.
G_K	quantity in the generation term for k.
I,J,K,L,M,N	radiation fluxes in the r, x and θ directions.
k	kinetic energy of turbulence.
ℓ	length scale of turbulence.
m_J	mass fraction of a species J.
m_{fu}, m_{ox}, m_{pr}	mass fractions of fuel, oxygen and product respectively.
p	pressure.
Q^x, Q^y, Q^z	net radiative transfer in the coordinate directions.
R_J	mass rate of creation of species J by chemical reaction.
R^x, R^y, R^z	a dependent variable for radiation fluxes in the three coordinate directions.
r	distance from axis of symmetry.
s	stoichiometric mass ratio.
S_1	scattering coefficient for radiation.
S_2	source term.
T	absolute temperature.
t	time.
u, v, w	velocity components in the x, r and z (or θ) directions.
$\vec{v}$	velocity vector.
x, z	coordinate distances.

KE_{av}	mean kinetic energy.
MT	total number of mixed gaseous species.
m	mass of reactor gas phase.
NT	total number of gaseous species.
n_j	temperature exponent in modified Arrhenius equation.
P	pressure.
$\dot{p}_i$	rate of production of species i by chemical reaction.
q	dynamic head.
R	univeral gas constant.
Re	Reynold's number of droplet.
r_L	droplet radius.
T	temperature.
T_L	temperature of droplet surface.
$\bar{U}$	mean velocity.
u'	fluctuating velocity.
V	reactor volume.
v_{rel}	velocity relative to droplet.
W_i	molecular weight of species i.
X_j	third body concentration in a dissociation reaction j.
α_{ij}	stoichiometric coefficient of species i as a product in reaction j.
β	$\dot{FE}/\dot{m}_2$ non-dimensionalized evaporation rate.
γ_i	mass fraction of species i in reactor mixed gas phase.
δ_{ij}	stoichiometric coefficient of species i as a reactant in reaction j.
ϵ	mass of reactor liquid phase.
λ	mean thermal conductivity of gas phase.
μ	viscosity.

Γ diffusion coefficient.

$\Gamma_{J,eff}$ effective exchange coefficient for J.

ε dissipation rate of turbulence.

μ viscosity.

ρ density.

σ Stefan-Boltzman constant.

ϕ general dependent variable.

θ coordinate in the cylindrical-polar system.

ii) Stirred Reactor equations.

A_j Pre-exponential factor of the jth reaction.

B_j Reverse reaction rate of the jth reaction.

b_j rate constant of the reverse of reaction j.

B_{ev} transfer number in evaporation rate equation $[\bar{C}_p(T-T_L)/L]$.

C_i overall gas phase mass fraction of ith species.

$\bar{C}_p$ mean heat capacity of gas phase.

C_D droplet drag coefficient.

D dissipation energy term.

d_{ij} third body efficiency of species i in reaction j (usually assumed to be 1).

E_j activation energy of the jth reaction.

$\dot{FE}$ fuel evaporation rate.

F_j forward reaction rate of reaction j.

F_i^o standard molar free energy of species i.

f_j forward rate constant of reaction j.

$\dot{H}_L$ rate of enthalpy loss from the reactor.

h_i specific enthalpy of species i.

K_j equilibrium constant of jth reaction.

ρ	density.
α_j	index to indicate whether the third body participates.
τ_D	characteristic dissipation time.
τ_s	reactor stay time.
τ_{SD}	τ_s/τ_D, unmixedness parameter.
ϕ_u	proportion of gas phase which is unmixed.
ω_i	mass fraction of species i in reactor unmixed gas phase.

Superscripts

i	feed conditions.
*	intermediate value (i.e. after mixing and evaporation).

Subscripts

1	reactor inlet.
2	reactor outlet.
G	gas phase.
L	liquid phase.
f	fuel.
N_2	nitrogen.
O_2	oxygen.
cs	general combustion species.
i	chemical species identifier.
j	chemical reaction identifier.
E	evaporation.
E,F	forced evaporation.

References

1. J. Swithenbank "Flame Stabilization in High Velocity Flow", Combustion Technology (Ed. Palmer and Beér), Academic Press, 1974, pp.91-125.

2. F. Boysan and J. Swithenbank "Spray Evaporation in Recirculating Flow", Dept. of Fuel Technology and Chemical Engineering, Report No. HIC 290, June, 1977.

3. Patankar S.V. and Spalding D.B.: "A calculation procedure for heat, mass and momentum transfer in three-dimensional parabolic flows", Int.J. Heat Mass Transfer, 15, pp.1787-1806, 1972.

4. Launder B.E. and Spalding D.B.: "The numerical computation of turbulent flows". Computer Methods in Applied Mechanics and Engineering, Vol.3, pp.269-289, 1974.

5. Spalding D.B. "Mixing and chemical reaction in steady confined turbulent flames", Thirteenth Symposium (International) on Combustion, 1971.

6. A.D. Gosman and F.C. Lockwood :"Incorporation of a flux model for radiation into a finite difference procedure for furnace calculation", Proc.14th Symposium (International) on Combustion, pp.661-671.

7. Gosman, A.D. and Pun, W.M.: Lecture Notes for course entitled "Calculation of Recirculating Flows", Imperial College of Science and Technology, December, 1973.

8. J. Swithenbank, I. Poll, D.D. Wright & M.W. Vincent, "Combustion Design Fundamentals",14th Combustion (Int.) Symposium, Pennsylvania, p.627, 1973.

9. I. Poll, "Chemical Reactor Modelling applied to Gas Turbine combustors", A.R.C. report No. 35883 (Comb.165), 1975.

10. I. Poll, R. Payne, J. Swithenbank and M.W. Vincent, Second International Symposium on Air Breathing Engines, Sheffield, 1974.

11. I.T. Osgerby, "An efficient numerical method for stirred reactor calculations", A.E.D.C. Report No. TR-72-164.

12. H. Wise et al., 5th Combustion (Int.) Symposium, p.32, 1955.

13. N. Frössling, "The evaporation of falling drops", Gerlands Beitrage Zur Geophysik, 52, p.170, 1938.

14. M.W. Vincent, "Fuel spray evaporation in gas turbine combustors", Ph.D. thesis, Sheffield, University, 1973.

15. J. Swithenbank et al., "A laser diagnostic for the measurement of droplet and particle size distribution", AIAA Paper No. 76-69.

16. I.G. Bowen & J.R. Joyce, Shell Technical Report No. ICT/17, 1948.

17. W. Tipler, "The measurement and significance of fuel spray momentum", Shell Technical Report No. APD 202/62M, 1962.

18. S.B. Pope, "The probability approach to modelling of turbulent reacting flows", Combustion & Flame, 27, 299-312, 1976.

Table 1. Summary of equations solved

Equation	ϕ	β	Γ	S_2
Continuity	1	ρ	0	0
x-momentum	u	ρ	μ	$-\frac{\partial p}{\partial x} + \frac{\partial}{\partial x}(\mu \frac{\partial u}{\partial x}) + \frac{1}{r}\frac{\partial}{\partial r}(r\,\mu \frac{\partial v}{\partial x}) + \frac{\partial}{r\partial\theta}(\mu \frac{\partial w}{\partial x})$
r-momentum	v	ρ	μ	$-\frac{\partial p}{\partial r} + \frac{\partial}{\partial x}(\mu \frac{\partial u}{\partial r}) + \frac{1}{r}\frac{\partial}{\partial r}(r\,\mu \frac{\partial v}{\partial r}) + \frac{1}{r}\frac{\partial}{\partial\theta}\left[\mu(\frac{\partial w}{\partial r}) - \frac{w}{r}\right] + \frac{\rho w^2}{r} - \frac{2\mu}{r}(\frac{\partial w}{r\partial\theta} + \frac{v}{r})$
θ-momentum	w	ρ	μ	$-\frac{\partial p}{r\partial\theta} + \frac{\partial}{\partial x}(\frac{\mu}{r}\frac{\partial u}{\partial\theta}) + \frac{1}{r}\frac{\partial}{\partial r}\left[\mu r(\frac{1}{r}\frac{\partial v}{\partial\theta} - \frac{w}{r})\right] - \frac{\rho vw}{r} + \frac{\partial}{r\partial\theta}\left[\frac{\mu}{r}(\frac{\partial w}{\partial\theta} + 2v)\right] + \frac{\mu}{r}(\frac{\partial w}{\partial r} + \frac{\partial v}{r\partial\theta} - \frac{w}{r})$
Turbulence energy	k	ρ	$\frac{\mu_{eff}}{\sigma_{k,eff}}$	$G_K - C_D\,\rho\epsilon$
Energy dissipation rate	ϵ	ρ	$\frac{\mu_{eff}}{\sigma_{\epsilon,eff}}$	$(C_1\,G_k - C_2\,\rho\epsilon)\,\epsilon/k$
Fuel Mass fraction	m_{fu}	ρ	$\frac{\mu}{\sigma_{fu}}$	R_{fu} depends on the case considered.
Composite mass fraction	f	ρ	$\frac{\mu}{\sigma_{fu\ ox}}$	0
Stagnation enthalpy	$\tilde{h}$	ρ	$\frac{\mu}{\sigma_n}$	1) 0, if no radiation; 2) $2a(R^x+R^y+R^z-3E)$ if radiation is included.
x-direction composite-radiation-flux	R^x	0	$\frac{1}{a + S_1}$	$-\frac{1}{r}\left[\frac{\partial}{\partial r}(\frac{r}{a+S_1}\frac{\partial R^x}{\partial r}) + \frac{\partial}{\partial\theta}(\frac{1}{a+S_1}\frac{\partial R^x}{r\partial\theta})\right] - \left[a(R^x-E) + \frac{S_1}{3}(2R^x - R^y - R^z)\right]$
r-direction composite-radiation-flux	R^y	0	$\frac{1}{a + S_1 + \frac{1}{r}}$	$-\frac{\partial}{\partial x}(\frac{1}{a + S_1 + \frac{1}{r}}\frac{\partial R^y}{\partial x}) - \frac{\partial}{r\partial\theta}(\frac{1}{a + S_1 + \frac{1}{r}}\frac{\partial R^y}{r\partial\theta} - \left[a(R^y - E) + \frac{S_1}{3}(2R^y - R^x - R^z)\right]$
θ-direction composite-radiation-flux	R^z	0	$\frac{1}{a + S_1}$	$-\frac{\partial}{\partial x}(\frac{1}{a + S_1}\frac{\partial R^z}{\partial x}) - \frac{1}{r}\frac{\partial}{\partial r}(\frac{r}{a + S_1}\frac{\partial R^z}{\partial r}) - \left[a(R^z - E) + \frac{S_1}{3}(2R^z - R^x - R^y)\right]$

TABLE 2. WSR COMBUSTION SCHEME

(1)	Liquid fuel	→ Evaporated fuel (unmixed)	EVAPORATION
(2)	Evaporated fuel (unmixed)	→ Evaporated fuel (mixed)	MIXING
	Oxygen (unmixed)	→ Oxygen (mixed)	
	Nitrogen (unmixed)	→ Nitrogen (mixed)	
(3)	Evaporated fuel (mixed) + Oxygen (mixed)	→ Combustion products	CHEMICAL REACTION
	Oxygen (mixed) + Nitrogen (mixed)		

Table 3 Kerosine Combustion, Reaction Mechanism

Reaction step	Forward reaction rate data A_j	E_j (cal/mole)	n_j
$C_{12}H_{24} + 6\ O_2 \rightarrow 12\ H_2 + 12\ CO$			
$CO + OH \rightleftharpoons CO_2 + H$	0.56×10^{12}	544	0
$H + O_2 \rightleftharpoons OH + O$	0.22×10^{15}	8450	0
$O + H_2 \rightleftharpoons OH + H$	0.18×10^{11}	4480	1
$OH + H_2 \rightleftharpoons H_2O + H$	0.219×10^{14}	2592	0
$OH + OH \rightleftharpoons H_2O + O$	0.575×10^{13}	393	0
$H + O + M \rightleftharpoons OH + M$	0.53×10^{16}	-2780	0
$H + OH + M \rightleftharpoons H_2O + M$	0.14×10^{24}	0	-2
$H + H + M \rightleftharpoons H_2 + M$	0.30×10^{16}	0	0
$O + O + M \rightleftharpoons O_2 + M$	0.47×10^{16}	0	-0.28
$N + O_2 \rightleftharpoons NO + O$	0.64×10^{10}	3150	1
$N_2 + O \rightleftharpoons NO + N$	0.76×10^{14}	38000	0
$N + OH \rightleftharpoons NO + H$	0.32×10^{14}	0	0
$N_2 + O + M \rightleftharpoons N_2O + M$	0.162×10^{12}	1601	0
$N_2O + O \rightleftharpoons NO + NO$	0.458×10^{14}	12130	0
$N_2O + O \rightleftharpoons N_2 + O_2$	0.381×10^{14}	12130	0
$N_2O + H \rightleftharpoons N_2 + OH$	0.295×10^{14}	5420	0

(Backward reaction rates evaluated from equilibrium constants obtained from free energy function)

Table 4 Full Model : Effect of air flowrate

WSR_2, $\tau_{SD} = 7$.

$P_f = 120$ psig, $T_{ROT} = 288K$

Model predictions and corresponding measured values :

BFB Conditions				WSR_1				WSR_2		Exit Flow (-90% H_2O)		Measured Exit Flow Composition		
T_{AIR} (K)	$\dot{Q}_j$ (1/min)	P_{cc} ("H_g)	ϕ_{OV}	ϕ_{WSR}	T_2 (K)	NO (ppm)	CO (%)	ϕ_{WSR}	T_2 (K)	NO (ppm)	CO (%)	T (K)	NO (ppm)	CO (%)
353	620	15.4	0.518	0.43	1216.6	0.56	0.45	0.50	1462.7	1.96	0.20	1480	1.2	-
353	500	8.0	0.704	0.62	1454.5	1.57	0.45	0.69	1699.4	4.48	0.33	1590	5.3	0.1
353	430	7.3	0.827	0.72	1601.7	2.30	0.65	0.81	1840.1	8.39	0.54	1675	14.4	0.4
353	370	5.2	0.990	0.89	1767.1	5.08	1.20	0.97	2007.8	20.2	1.35	1765	28.0	1.55

Table 5 Full Model : Effect of P_f on pollutant emissions

WSR_2 $\tau_{SD} = 7$

BFB conditions : $\dot{Q}_j = 430$ lit/min, $P_{cc} = 7.3$" Hg, $T_{ROT} = 288K$

Model predictions and corresponding measured values :

			WSR_1				WSR_2		EXIT FLOW (-90% H_2O)		MEASURED EXIT FLOW COMPOSITION		
P_f (psig)	T_{AIR}	ϕ_{OV}	ϕ_{WSR}	T_2 (K)	NO (ppm)	CO (%)	ϕ_{WSR}	T_2 (K)	NO (ppm)	CO (%)	T (K)	NO (ppm)	CO (%)
80	353	0.710	0.59	1433.2	1.78	0.38	0.69	1723.6	5.76	0.35	1570	5.2	-
100	353	0.776	0.68	1533.8	2.08	0.51	0.76	1791.2	7.03	0.44	-	-	0.15
120	453	0.827	0.74	1643.4	2.96	0.69	0.81	1876.7	11.35	0.57	1675	14.4	0.4
140	553	0.865	0.79	1710.7	4.26	0.83	0.85	1954.8	19.70	0.76	-	-	0.7
160	653	0.893	0.83	1779.5	6.71	1.04	0.88	2009.0	29.07	0.90	1830	35.0	1.2

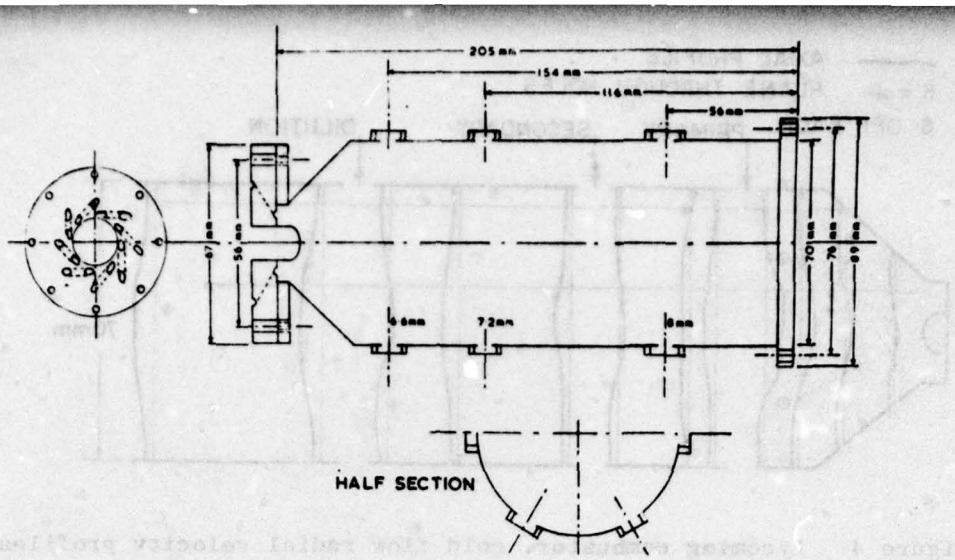

Figure 1. Gas Turbine combustor can (Lycoming)

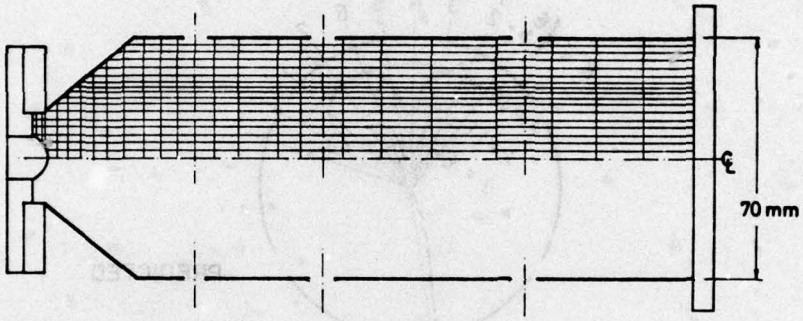

Figure 2. Finite difference grid for the combustor.

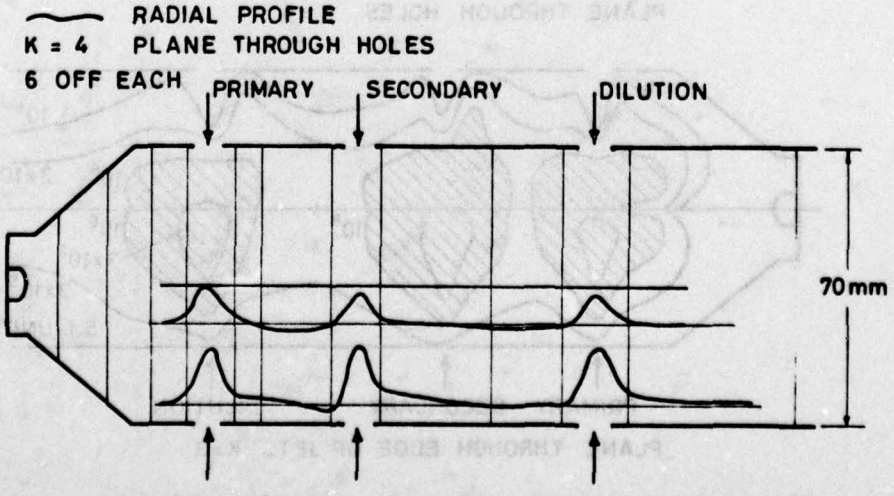

Figure 3. Lycoming combustor, cold flow radial velocity profiles axial cross-section.

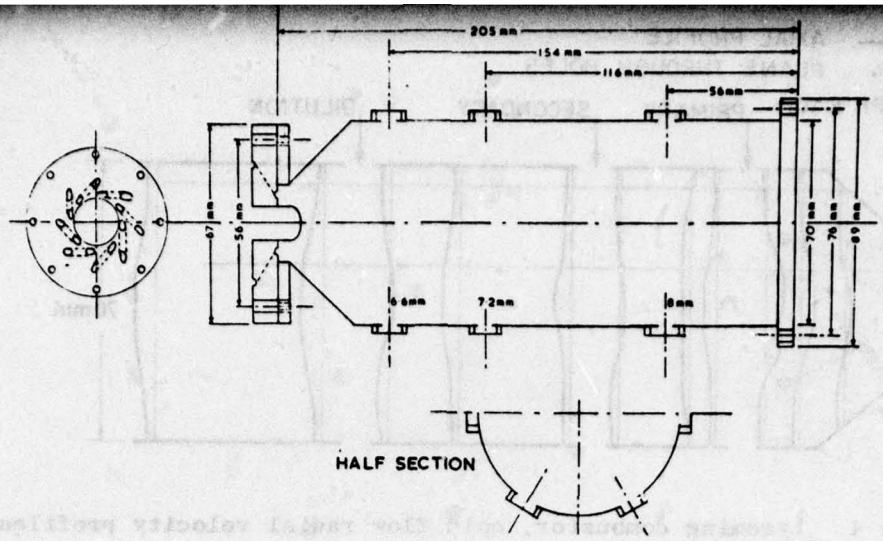

Figure 1. Gas Turbine combustor can (Lycoming)

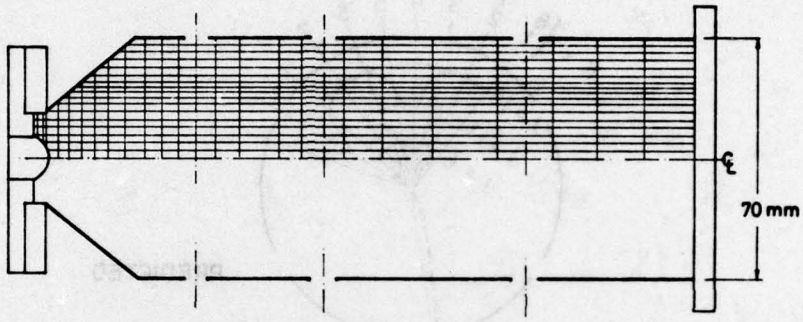

LYCOMING COMBUSTOR,
GRID ARRANGEMENT 27 x 18 x 7 = 3402 TOTAL POINTS

Figure 2. Finite difference grid for the combustor.

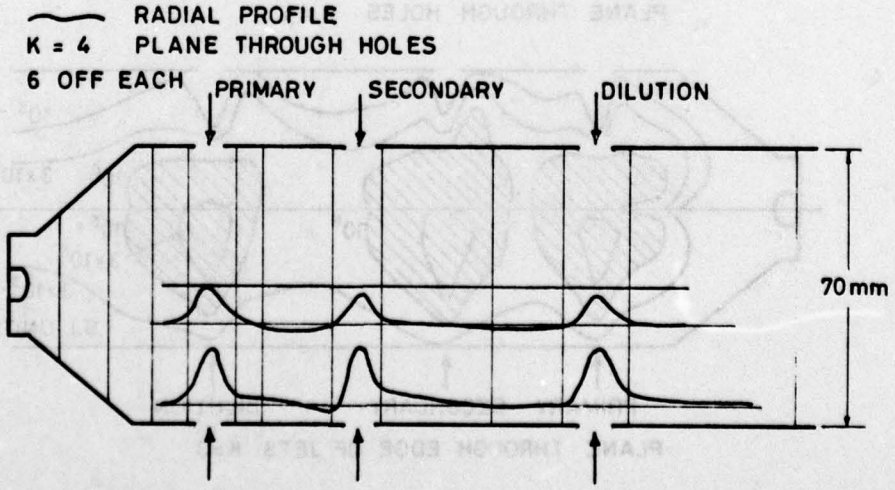

Figure 3. Lycoming combustor, cold flow radial velocity profiles axial cross-section.

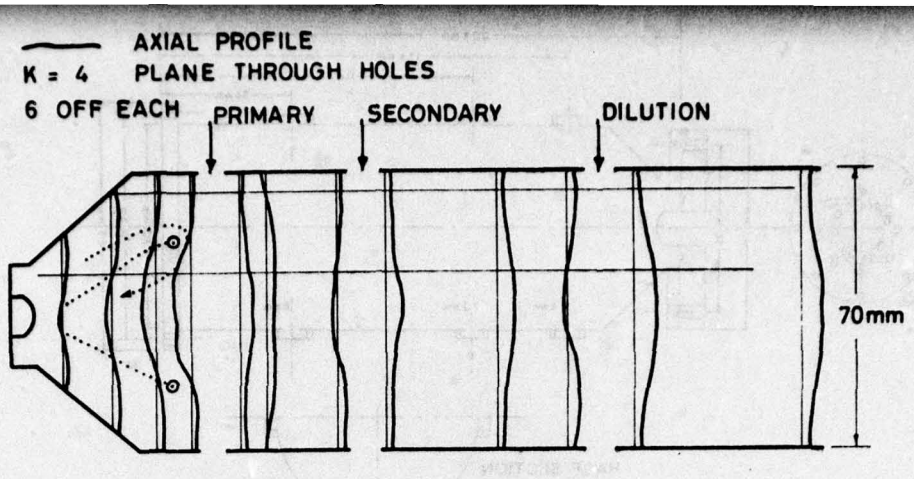

Figure 4. Lycoming combustor, cold flow radial velocity profiles axial cross-section.

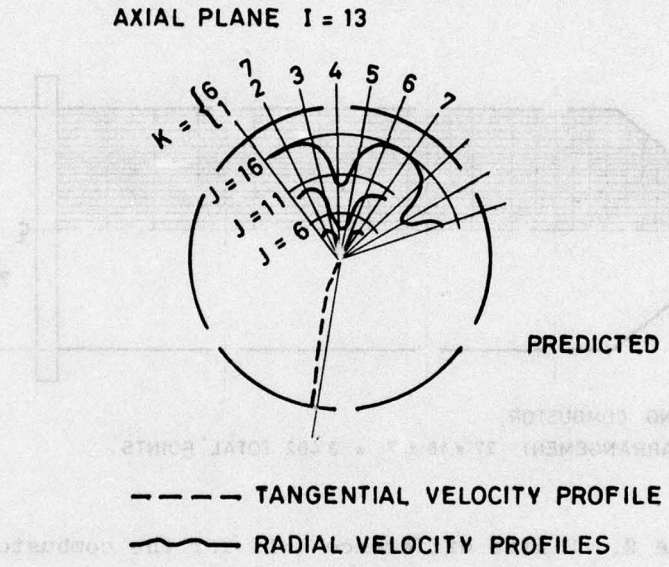

Figure 5. Lycoming combustor, cold flow radial and tangential velocity profiles, transverse cross-section.

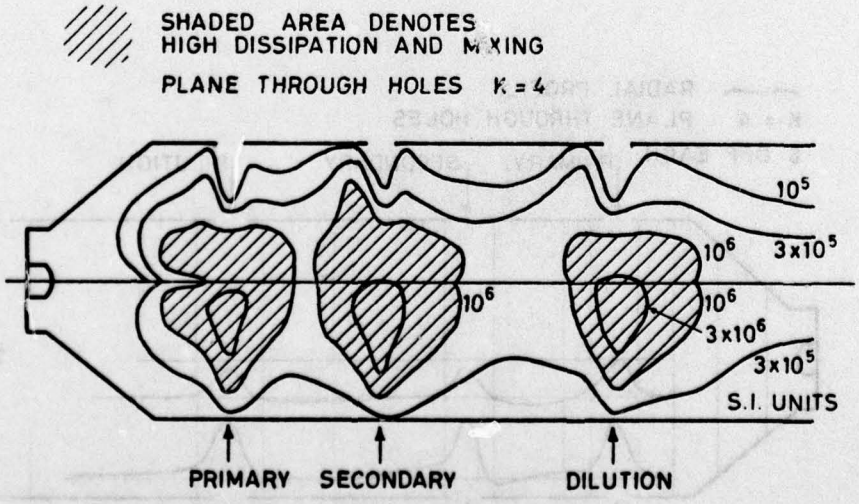

Figure 6. Lycoming combustor, cold flow turbulence dissipation (ε) axial cross-sections.

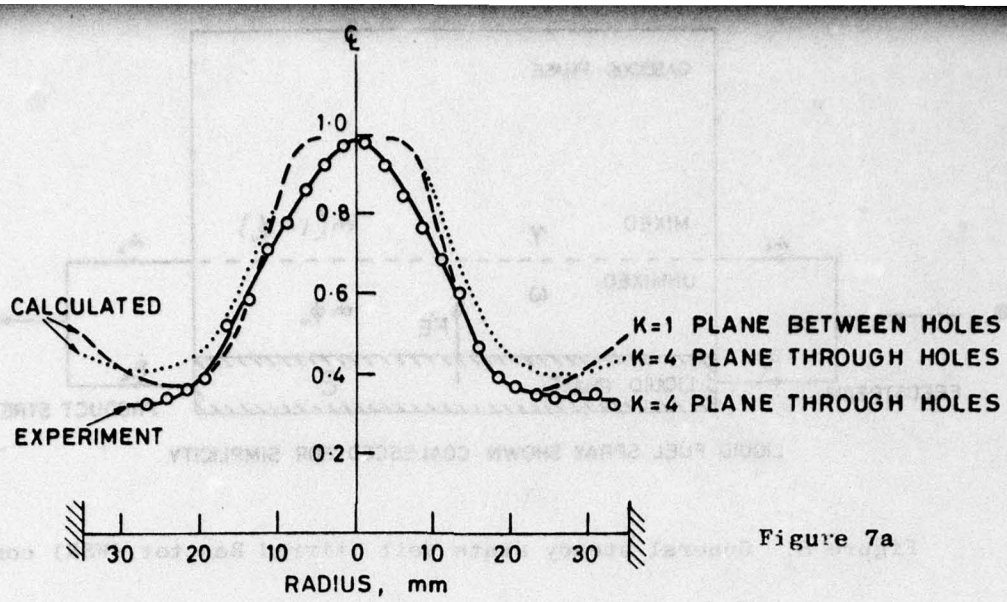

Figure 7a

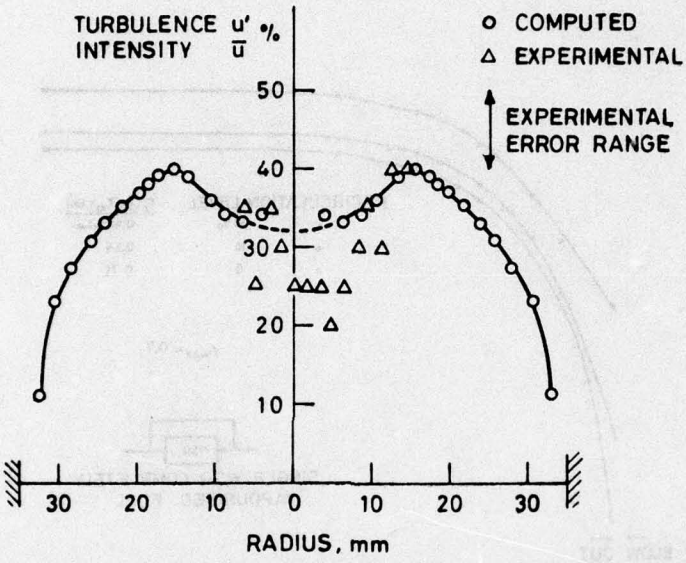

Figure 7b

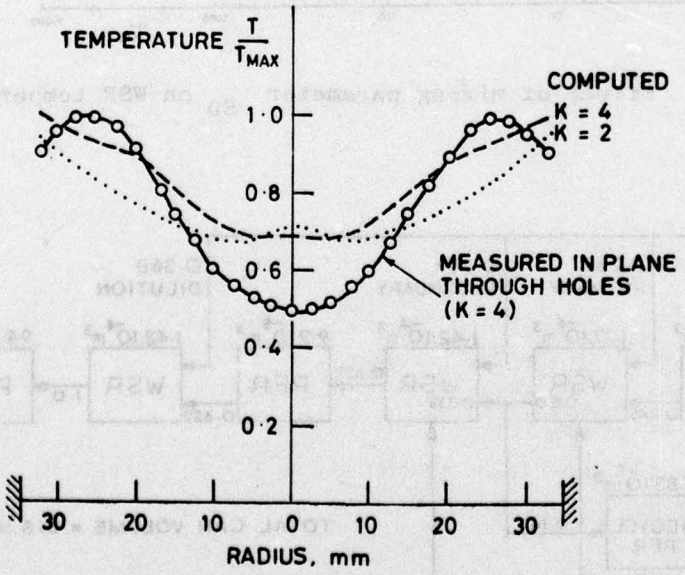

Figure 7c

Figure 7a Lycoming combustor, cold exit velocity profiles - predicted and measured.

Figure 7b Lycoming combustor, exit turbulence intensity profiles with combustion, predicted and measured with photon correlation anemometer.

Figure 7c Lycoming combustor, exit temperature profiles with combustion, predicted and measured.

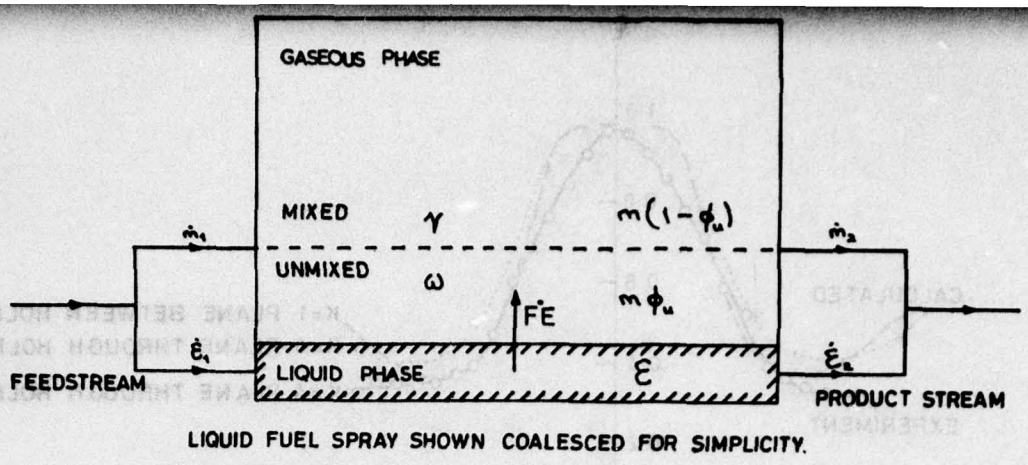

Figure 8. General steady state Well Stirred Reactor (WSR) composition.

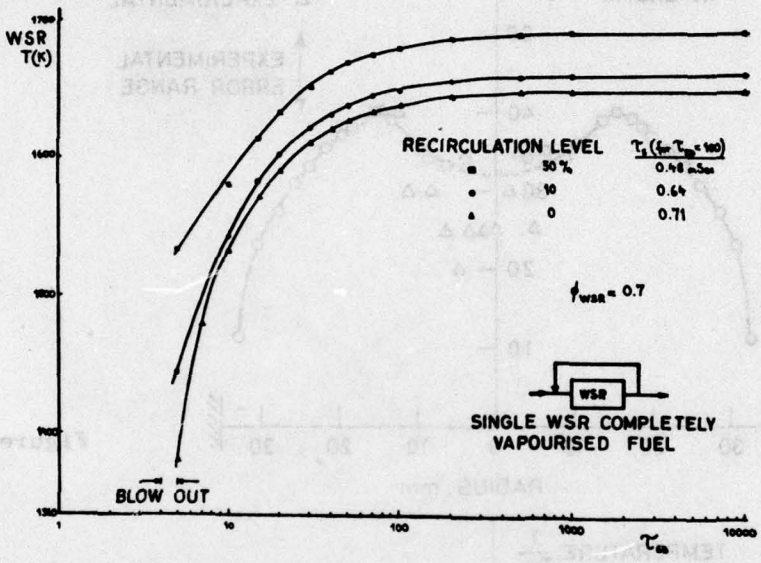

Figure 9. Effect of mixing parameter τ_{SD} on WSR temperature.

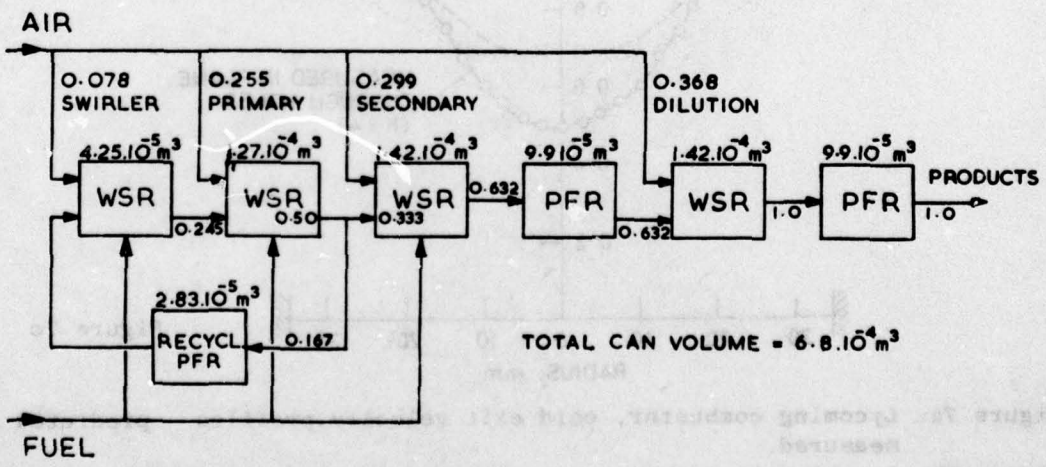

Figure 10. Gas turbine combustor, typical interconnection of reactors comprising reactor network model.

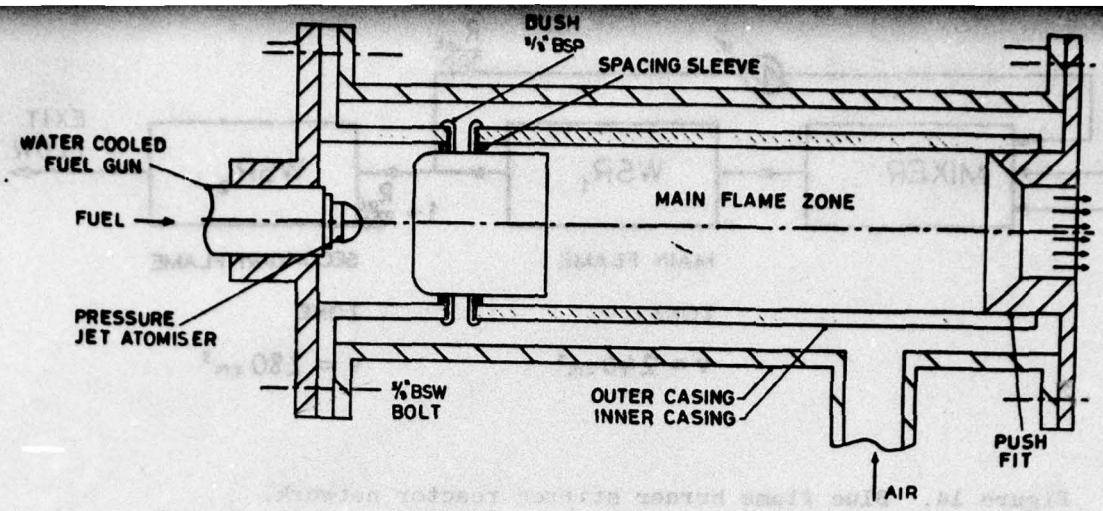

Figure 11. Sectional view of the blue flame combustor, axisymmetric.

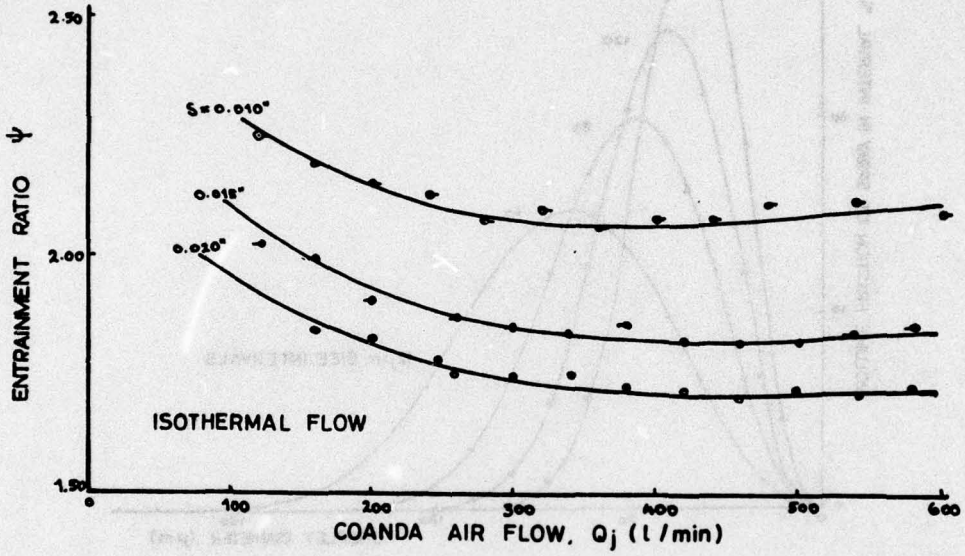

Figure 12. Measured coanda characteristic: ejector entrainment ratio.

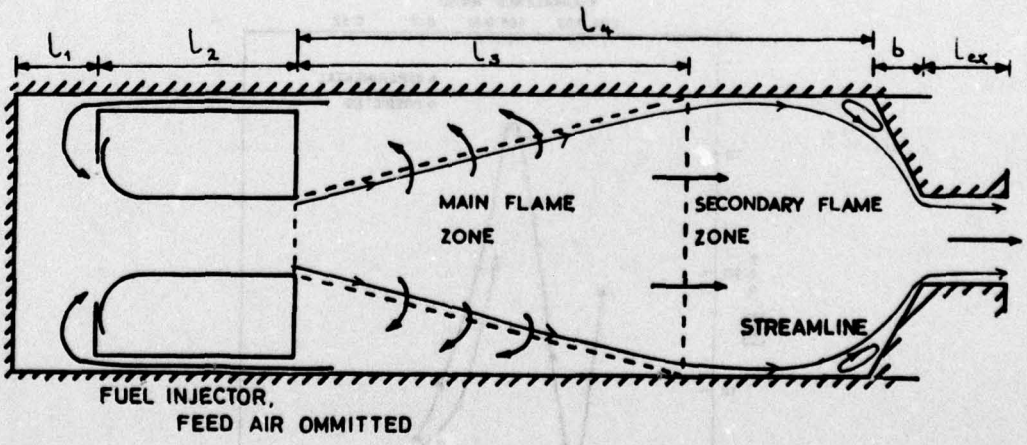

Figure 13. Blue flame burner schematic representation of flame zones.

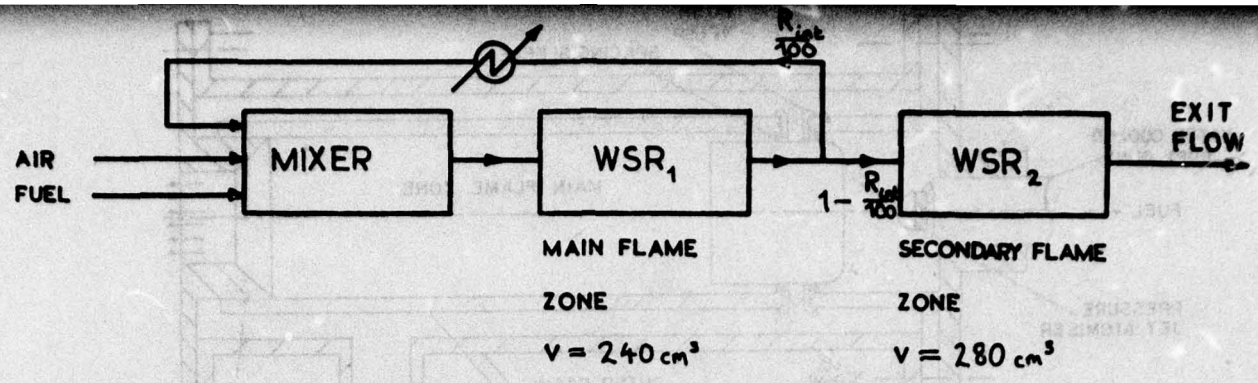

Figure 14. Blue flame burner stirred reactor network.

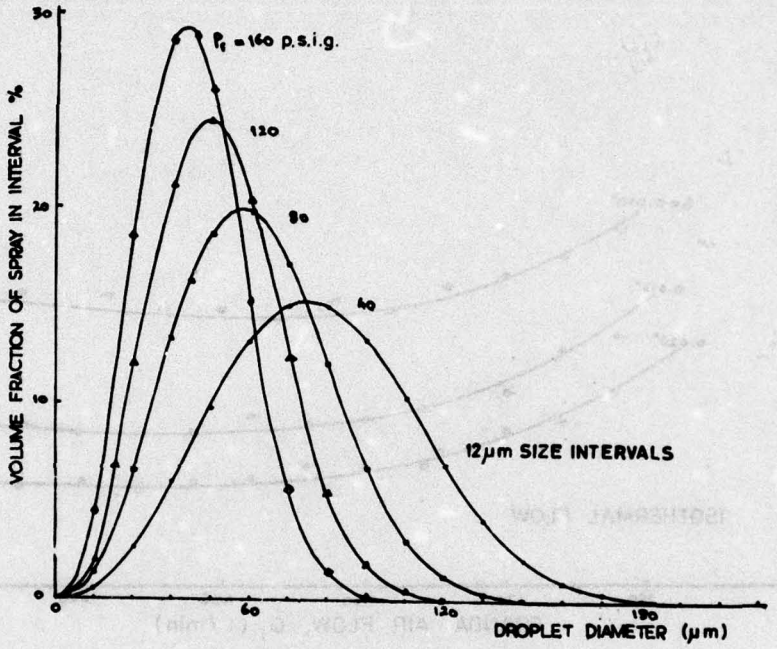

Figure 15. Measured atomizer initial dropsize distribution characteristics.

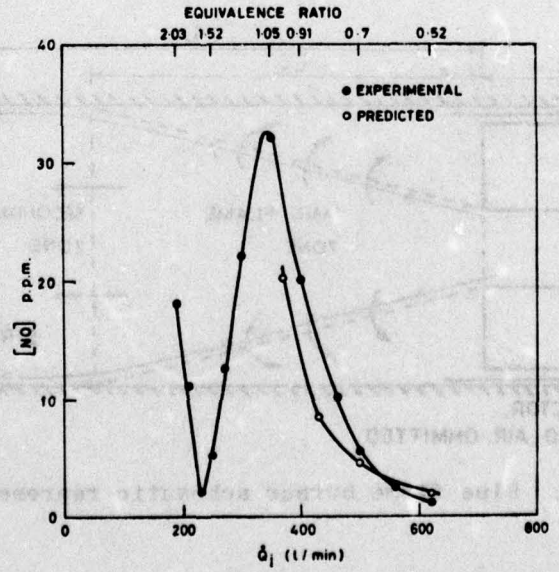

Figure 16. Burner exit Nitric Oxide concentrations, Measured and predicted, vs air flow rate.

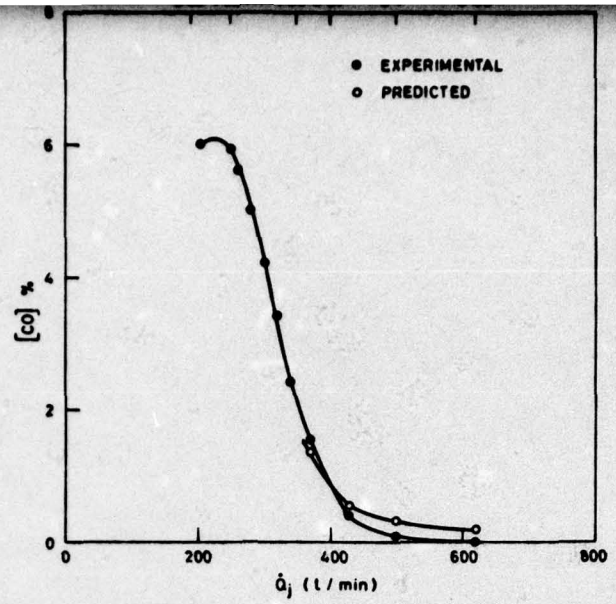

Figure 17.
Burner exit Carbon Monoxide concentration vs air flow rate. Measured and predicted.

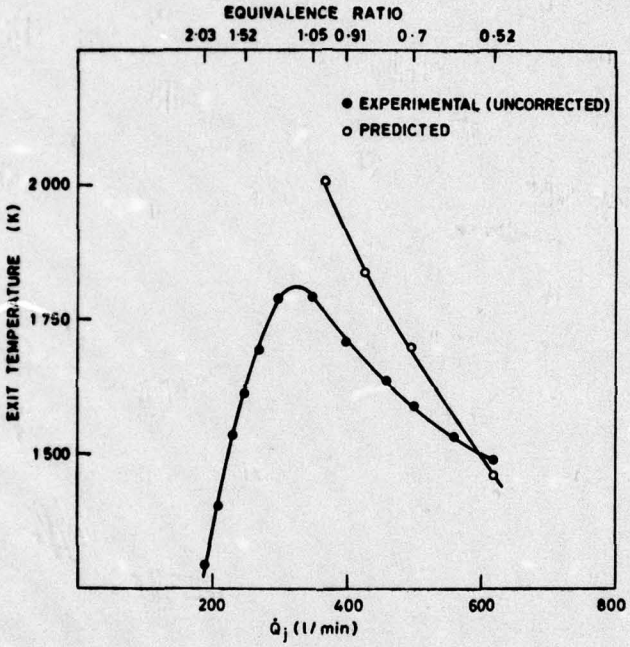

Figure 18.
Burner exit temperature vs air flow. Predicted and uncorrected experimental values.

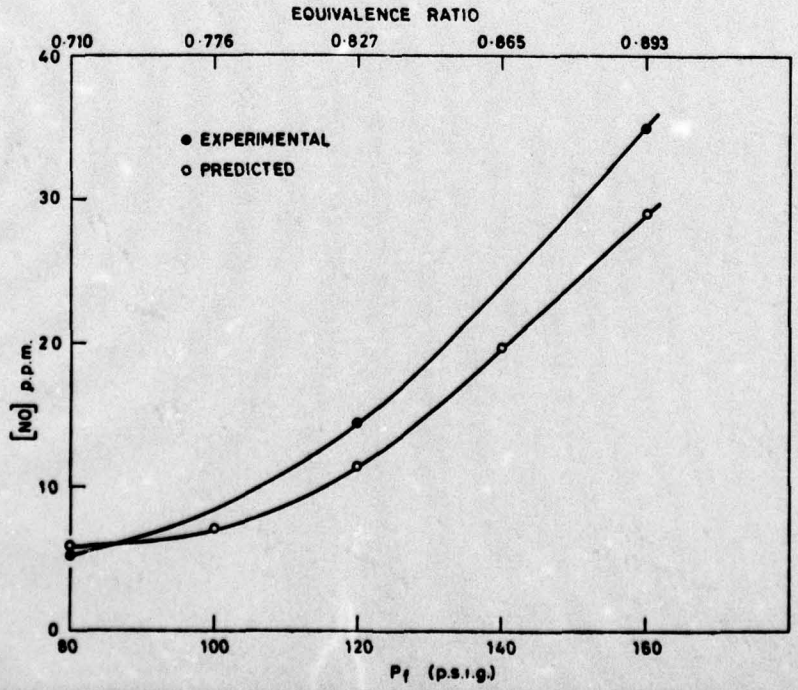

Figure 19.
Burner exit, effect of fuel pressure (flowrate and drop size) on Nitric Oxide production.

SECURITY CLASSIFICATION OF THIS PAGE (When Data Entered)

REPORT DOCUMENTATION PAGE

READ INSTRUCTIONS BEFORE COMPLETING FORM

1. REPORT NUMBER: AFOSR-TR-77-1297	2. GOVT ACCESSION NO.
3. RECIPIENT'S CATALOG NUMBER	
4. TITLE (and Subtitle): PROGRESS IN MODELLING COMBUSTORS.	5. TYPE OF REPORT & PERIOD COVERED: INTERIM progress report no. 11, 1 Mar [redacted] — 31 Aug 77,
6. PERFORMING ORG. REPORT NUMBER: SR[redacted]2 [redacted] HIC-3001	
7. AUTHOR(s): P. G. FELTON, J. SWITHENBANK, A. TURAN	8. CONTRACT OR GRANT NUMBER(s): AFOSR-74-2682
9. PERFORMING ORGANIZATION NAME AND ADDRESS: UNIVERSITY OF SHEFFIELD, CHEMICAL ENGINEERING & FUEL TECHNOLOGY DEPT, SHEFFIELD S13JD ENGLAND.	10. PROGRAM ELEMENT, PROJECT, TASK AREA & WORK UNIT NUMBERS: 2308A2, 61102F
11. CONTROLLING OFFICE NAME AND ADDRESS: AIR FORCE OFFICE OF SCIENTIFIC RESEARCH/NA, BLDG 410, BOLLING AIR FORCE BASE, D C 20332	12. REPORT DATE: 1977
	13. NUMBER OF PAGES: 42
14. MONITORING AGENCY NAME & ADDRESS (if different from Controlling Office): 45 P.	15. SECURITY CLASS. (of this report): UNCLASSIFIED
	15a. DECLASSIFICATION/DOWNGRADING SCHEDULE

16. DISTRIBUTION STATEMENT (of this Report)

Approved for public release; distribution unlimited.

17. DISTRIBUTION STATEMENT (of the abstract entered in Block 20, if different from Report)

18. SUPPLEMENTARY NOTES

19. KEY WORDS (Continue on reverse side if necessary and identify by block number)

MODELING
COMBUSTION
SPRAYS
STIRRED REACTORS
TWO-PHASE FLOW
COMBUSTION EFFICIENCY
FINITE DIFFERENCE
NAVIER STOKES

20. ABSTRACT (Continue on reverse side if necessary and identify by block number)

Recent advances in the solution of the problem of predicting the performance of combustors have been based on finite difference and stirred reactor methods. Due to the limitations of present computers finite difference methods cannot be extended to completely include fuel spray dynamics and realistic chemical kinetics. This difficulty is overcome by using the computed flow patterns to define a network of interconnected stirred and plug-flow reactors. The detailed kinetic scheme presently consists of 13 species undergoing 18 reactions to represent the combustion of hydrocarbon fuels such as kerosine. A model of fuel evaporation

DD FORM 1 JAN 73 1473 EDITION OF 1 NOV 65 IS OBSOLETE

UNCLASSIFIED

SECURITY CLASSIFICATION OF THIS PAGE (When Data Entered)

400 047

is incorporated which assumes the fuel spray to be composed of 21 x 12 μm size ranges, evaporation is calculated using a forced convection model. The mixing of fuel vapour and air is modelled using a micro-mixing parameter, τ_{SD}, based on turbulence dissipation rates. The over-all method thus combines 3-D fluid dynamics, turbulent mixing, evaporation and chemical kinetics. The model has been varified by experiments which show that flow velocity profiles, chemical species (CO,NO etc) can be successfully computed.